Pressure–Slope Momentum Transfer in Ocean Surface Boundary Layers Coupled with Gravity Waves

GEORGE MELLOR

Program in Atmospheric and Oceanic Sciences, Princeton University, Princeton, New Jersey

(Manuscript received 28 March 2013, in final form 27 June 2013)

ABSTRACT

The paper focuses on the consequences of including surface and subsurface, wind-forced pressure–slope momentum transfer into the oceanic water column, a transfer process that competes with now-conventional turbulence transfer based on mixing coefficients. Horizontal homogeneity is stipulated as is customary when introducing a new surface boundary layer model or significantly new vertical momentum transfer physics to an existing model. An introduction to pressure–slope momentum transfer is first provided by a phase-resolved, vertically dependent analytical model that excludes turbulence transfer. There follows a discussion of phase averaging; an appendix is an important adjunct to the discussion. Finally, a coupled wave–circulation model, which includes pressure–slope and turbulence momentum transfer, is presented and numerically executed. The calculated temperatures compare well with measurements from ocean weather station Papa.

1. Introduction

Previous to this paper, surface boundary layer models (e.g., Mellor and Yamada 1982; Large et al. 1994) generally assumed that momentum transfer from surface wind stress into the water column is due to turbulence Reynolds stress. Here, we examine the finding of Mellor [(2003), a corrected version can be found in ftp://aden.princeton.edu/pub/glm/corrected2003] that waves create a contribution as a result of the correlation of wind pressure and wave slope, also called form drag, which is projected into the water column and competes with turbulence-supported stress. It is noted that form drag also penetrates into the atmosphere, but by a small distance relative to atmospheric boundary layer heights; it has played a role in drag coefficient parameterizations (e.g., Hwang 2006).

To focus on vertical transfer processes, most surface boundary layer models are initiated assuming horizontal homogeneity wherein the model algorithm and the relevant empiricism are introduced and tested against available data. Because this paper examines a new element of surface wave boundary layer physics, horizontal homogeneity will also be assumed.

In section 2, a phase-resolved analytical solution of a stationary, wind-forced wave field in the absence of turbulence is developed. Surface wind pressure penetrates the water column. Then, in section 3, after phase averaging the information of section 2, it is seen that momentum is transferred into the water column entirely because of wave pressure acting on sloping material surfaces resulting in Stokes drift. When interpreted in terms of surfaces of constant z rather than material surfaces, a nonzero wave correlation $\widetilde{\widetilde{u}\widetilde{w}}$ is obtained.

In section 4, a model, again specialized for horizontal homogeneity but including waves, currents, and turbulence, is presented and executed numerically. The interplay between pressure–slope- and turbulence-supported momentum transfer is demonstrated. For the turbulence portion, an augmented Mellor and Yamada (1982) model will be used. For the wave portion of the complete model, we will use the wave model developed by Mellor et al. (2008, hereafter MDO). Because horizontal homogeneity is prescribed, elements such as wave radiation stress terms are absent.

Comparisons with temperature data from station Papa (Martin 1985) are in section 5. There is uncertainty associated with the assumption of horizontal homogeneity because possible effects of advection are excluded.

Corresponding author address: George Mellor, Program in Atmospheric and Oceanic Sciences, Sayre Hall, Forrestal Campus, Princeton University, Princeton, NJ 08540.
E-mail: glmellor@princeton.edu

DOI: 10.1175/JPO-D-13-068.1

Of course, there are also uncertainties associated with the empirical content of all models.

2. A simple phase-resolved wave model

In this section, an analytical solution is obtained for a phase-resolved problem relevant to near-stationary (fully developed) waves wherein surface forcing is balanced by a simple momentum sink. The focus is on determining the subsurface pressure distribution and the effect of wind on wave properties.

For small wave slope, the linear equations of motion are

$$\frac{\partial u}{\partial x}+\frac{\partial w}{\partial z}=0, \tag{1}$$

$$\frac{\partial u}{\partial t}+\frac{\partial p}{\partial x}=-ru, \quad \text{and} \tag{2a}$$

$$\frac{\partial w}{\partial t}+\frac{\partial p}{\partial z}=-g-rw, \tag{2b}$$

where t is time; (x, z) is the horizontal and vertically upward coordinates respectively; (u, w) are the velocity components in the (x, z) directions; p is kinematic pressure (dynamic pressure divided by density); g is the gravity constant; and r is a simple, constant coefficient for Rayleigh drag that, it will be seen, counterbalances form drag. To simplify nomenclature and because mean properties will be horizontally homogeneous, we let the mean water level be nil.

From (2a) and (2b), one deduces irrotationality and, therefore, $(u, w)=(\partial\phi/\partial x, \partial\phi/\partial z)$. Also from (2)

$$\frac{\partial\phi}{\partial t}+gz+p=-r\phi. \tag{3}$$

We seek solutions whereby the surface elevation is $\eta=a\cos(kx-\sigma t)$, and where a, σ, and k are wave amplitude, frequency, and wavenumber, respectively. At the surface,

$$\frac{\partial\phi}{\partial z}=\frac{\partial\eta}{\partial t} \quad \text{for} \quad z=0. \tag{4}$$

In (4), small elevation is assumed (or $ka\ll 1$) so that $\phi(\eta)=\phi(0)+\phi_z(0)\eta+\cdots\cong\phi(0)$. At the bottom,

$$\frac{\partial\phi}{\partial z}=0 \quad \text{for} \quad z=-h. \tag{5}$$

After insertion of $(u, w)=(\partial\phi/\partial x, \partial\phi/\partial z)$ into (1), Laplace's equation is obtained for which a solution satisfying (4) and (5) is

$$\phi=\frac{a\sigma}{k}\frac{\cosh k(h+z)}{\sinh kh}\sin\psi \quad \text{and} \tag{6a}$$

$$\psi\equiv kx-\sigma t. \tag{6b}$$

According to (3),

$$p(z)=-gz+\frac{a\sigma^2}{k}\frac{\cosh k(h+z)}{\sinh kh}\left(\cos\psi-\frac{r}{\sigma}\sin\psi\right). \tag{7}$$

It is assumed that r/σ is small and that a possible $\cos\psi$ component of the wind surface pressure is similarly small;[1] thus, from (7) for $z=\eta$ and to lowest order in r/σ, one obtains the dispersion relation

$$\sigma^2=kg\tanh kh. \tag{8}$$

Let $p_w\equiv-(r/\sigma)ag\sin\psi$, so that (7) may be written

$$p=-gz+gF_{\mathrm{CC}}a\cos\psi+p_wF_{\mathrm{CC}}, \tag{9}$$

which uses (8) and the definition $F_{\mathrm{CC}}\equiv\cosh k(h+z)/\cosh kh$. For $p_w\propto r/\sigma\ll 1$, the flow is dominated by the standard, linear problem for zero surface pressure [for $z=\eta$ the first two terms on the right-hand side of (9) cancel]; the linear dispersion relation prevails and the (small) pressure component of the wind p_w is correlated with the surface elevation slope $\partial\eta/\partial x=-ka\sin\psi$.

3. Phase-averaged equations

The term p_wF_{CC} in (9) is the subsurface projection of the surface wind pressure as in Mellor (2003). The material surface ($z=\eta$) and subsurface departure from the rest is $\tilde{s}=aF_{\mathrm{SS}}\cos\psi$ (obtained from $\partial\tilde{s}/\partial t=w=\partial\phi/\partial z$), where $F_{\mathrm{SS}}\equiv\sinh k(z+h)/\sinh kh$.

Next, multiply (9) by the material slope $\partial\tilde{s}/\partial x=-kaF_{\mathrm{SS}}\sin\psi$. After phase averaging, one obtains

$$\tau_P\equiv\overline{p_wF_{\mathrm{CC}}\frac{\partial s}{\partial x}}=\overline{p_w\frac{\partial\eta}{\partial x}}F_{\mathrm{SS}}F_{\mathrm{CC}} \tag{10}$$

for the wave pressure–slope stress throughout the water column; at the surface, $F_{\mathrm{SS}}F_{\mathrm{CC}}=1$ and thus, (10) conforms to the well-known surface form drag $\tau_P(0)=\overline{p_w\partial\eta/\partial x}$. The term, form drag, is actually a drag on the atmospheric side of the air–sea interface; on the water

[1] It is small. From (10), (14), and calculations in section 5 (or from most any data source), one evaluates $r/\sigma=(860)^{-1}C_DU^2/kE\approx O(10^{-4})$. Originally, the problem was expanded in the small parameter $\varepsilon=r/\sigma\ll 1$, but this was subsequently deemed to overly complicate the discussion.

side it is a positive stress. In any event, form drag results from a greater integrated pressure on the backward face of a wave than on the forward face (e.g., Buckles et al. 1984); this is related to separated flow (the sheltering effect) or to aerodynamic boundary layer behavior for accelerating and decelerating velocities in attached flow.

For the present, horizontally homogeneous problem and following Mellor (2003), the phase-averaged momentum equation obtained from (2a), as derived in appendix A, is

$$\frac{\partial u_S}{\partial t} = \frac{\partial \tau_P}{\partial z} - r u_S. \tag{11}$$

This may seem intuitive but, in fact, its derivation is not too simple.

It can be shown and it is well known [in the introduction to Mellor (2003) there is a derivation that can serve as an introduction to the basic methods of that paper and appendix A] that the Stokes drift is

$$u_S = \frac{E}{c} \frac{\partial F_{\rm SS} F_{\rm CC}}{\partial z}, \tag{12}$$

where $E = g\overline{\eta^2} = ga^2/2$ is the wave energy, and c is the phase speed. After inserting (10) and (12) into (11), the vertically dependent parts of both sides of (11) cancel identically so that

$$\frac{\partial E}{\partial t} = c\overline{p_w \frac{\partial \eta}{\partial x}} - rE. \tag{13}$$

Alternately, if one multiplies (2a) by u, (2b) by w, adds the two equations, integrates from $z = -h$ to 0, phase averages, and makes further manipulation, one obtains (13) again. For the present problem of section 2, $\partial E/\partial t = 0$ and (13) yields

$$E = \frac{c}{r}\overline{p_w \frac{\partial \eta}{\partial x}}. \tag{14}$$

Thus, as might be anticipated, the wave energy is linearly proportional to the surface form drag and inversely proportional to the Rayleigh drag coefficient.

Whereas the Rayleigh terms, the second terms on the right of (11) and (12), are a convenient invention and differ from reality as seen in section 4, the first terms are derived from (1) and (2a) and (2b) exclusive of the Rayleigh terms and are considered realistic. Note also that here the momentum and energy equations are not independent.

At this point, it is useful to note that measurements taken at a fixed level instead of following a material surface should yield

$$\tau_P = \overline{p_w \frac{\partial \eta}{\partial x}} F_{\rm SS} F_{\rm CC} = -\overline{\tilde{u}\tilde{w}}. \tag{15}$$

(Henceforth, wave properties will be denoted by the superimposed symbol ~.) To arrive at (15), first note that the average momentum flux across any surface is given by $\mathbf{F} = L^{-1}\int_0^L (p\mathbf{n} + \mathbf{u}\mathbf{u}_r \cdot \mathbf{n})\, ds$, where ds is an elemental surface area whose normal unit vector is $\mathbf{n}$. The vector velocity on the surface is $\mathbf{u}$ whereas $\mathbf{u}_r$ is velocity relative to a moving surface. On a wave surface, $\mathbf{n} = -[1 - (\partial\tilde{s}/\partial x)^2]^{1/2}\mathbf{k} + \partial\tilde{s}/\partial x\mathbf{i}$ and $\mathbf{u}_r \cdot \mathbf{n} = 0$. If L is a wavelength, the x component of the momentum flux is $\mathbf{i} \cdot \mathbf{F} = \tau_P = \overline{p\partial\tilde{s}/\partial x}$ as in (15). On the other hand, for a fixed surface, $\mathbf{n} = -\mathbf{k}$, $\mathbf{u}_r \cdot \mathbf{n} = -\tilde{w}$, and $\mathbf{i} \cdot \mathbf{F} = \tau_P = -\overline{\tilde{u}\tilde{w}}$ as in (15).

4. A phase-averaged coupled wave–current model

The foregoing theoretical analysis introduced the idea of momentum transfer into the water column through pressure acting on material surfaces in the absence of turbulence transfer. In the following, the gradient $\partial\tau_P/\partial z$ will compete with the vertical turbulence stress gradient; the latter had been assumed to be the total stress in previous ocean surface, boundary layer models. As stated in the introduction, horizontal homogeneity is stipulated. For a horizontally variable application of the model see Mellor (2013).

a. The mean or total momentum equation

In this and the following subsections, the turbulence closure model of Mellor and Yamada (1982) is modified to include pressure–slope forcing and the inclusion of wave properties in surface boundary conditions. Another paper is relevant: in Mellor (2001), an extensive summary of the model is presented and a litany of problems is included, other than the surface boundary layer problem, for which the model has been applied.

The momentum equation is

$$\frac{\partial U_\alpha}{\partial t} - f\varepsilon_{\alpha\beta z}U_\beta = \frac{\partial \tau_{P\alpha}}{\partial z} + \frac{\partial \tau_{T\alpha}}{\partial z} - c_R \hat{u}_\alpha, \tag{16}$$

where, as derived in Mellor (2003), $U_\alpha = \hat{u}_\alpha + u_{S\alpha}$; $\hat{u}_\alpha$ is the current; $u_{S\alpha}$ is the Stokes drift; f is the Coriolis parameter; and $\varepsilon_{\alpha\beta z}$ is the permutation tensor (=1 if $\alpha\beta z = xyz$, $= -1$ if $\alpha\beta z = yxz$, or $= 0$ if $\alpha\beta z = xxz$ or yyz). The subscript α or β denotes horizontal coordinates x or y, whereas z is the vertical coordinate pointing upward from the sea surface. In (16) the turbulence stress term is $\tau_{T\alpha} = \overline{-u'_\alpha w'}$, where primes denote turbulence velocities. Note that turbulence is defined such that turbulent fluctuations are uncorrelated with wave motions; for

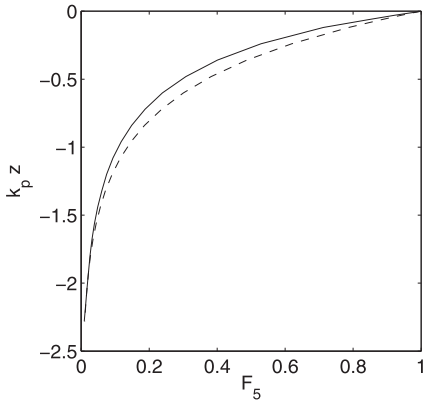

FIG. 1. Nondimensional $F_5(k_P z)$ as used in (17), applicable to deep water. The wave number at the peak frequency is given by k_P. The solid line is the spectral average of $F_{CC}F_{SS} = \exp(2kz)$, whereas the dashed line is simply $\exp(2k_P z)$. The max difference is about 25%.

example, $\overline{\tilde{u}_\alpha w'} = \overline{u'_\alpha \tilde{w}} = 0$. The Rayleigh-damping term $c_R \hat{u}_\alpha$ is necessary in one-dimensional calculations (Pollard and Millard 1970) lest the ocean velocities grow inexorably; it is a surrogate for missing three-dimensional processes. This artificial growth was demonstrated analytically and numerically in Mellor (2001) and where the value $c_R = (8\,\text{days})^{-1}$ was justified.

According to section 2, Mellor (2003), and Mellor et al. (2008), the wind-driven stress is

$$\tau_{P\alpha} = \overline{\tilde{p}_w \frac{\partial \tilde{\eta}}{\partial x_\alpha}} F_5(k_P z), \tag{17}$$

implemented here for the first time when modeling surface boundary layers. In the following, we specialize to deep water ($kh \gg 1$), wherein F_5 is the spectral average of $F_{CC}F_{SS} = \exp(2kz)$ plotted in Fig. 1 and is one of several averaged functions defined in Mellor et al. (2008). As in sections 2 and 3, $\tilde{p}_w$ is surface wind pressure correlated with the elevation slope $\partial\tilde{\eta}/\partial x_\alpha$.

The turbulence contribution to the momentum equation is

$$\tau_{T\alpha} = K_M \frac{\partial \hat{u}_\alpha}{\partial z}, \tag{18}$$

where K_M is a mixing coefficient defined below. Note that it is the current $\hat{u}_\alpha = U_\alpha - u_{S\alpha}$ that is used in (18) rather than U_α. This follows from the fact that attenuation of waves and therefore Stokes drift is governed by the wave energy equation [see (29) and (35)] rather than the momentum equation. Also, in the case of swell, waves and therefore Stokes drift attenuate very little (Snodgrass et al. 1966).

The vertical boundary conditions for (16) are

$$\tau_{P\alpha}(0) = \overline{\tilde{p}_w \frac{\partial \tilde{\eta}}{\partial x_\alpha}} = \varepsilon C_{DP} |\delta \mathbf{U}_{10}| \delta U_{10\alpha} \quad \text{and} \tag{19}$$

$$\tau_{T\alpha}(0) = \varepsilon C_{DT} |\delta \mathbf{U}_{10}| \delta U_{10\alpha}. \tag{20}$$

Here, $\delta \mathbf{U}_{10\alpha}$ is the difference between the 10-m wind vector and the ocean surface velocity; $\delta U_{10\beta} = |\delta \mathbf{U}_{10}|$ and $\varepsilon \cong 1/860$ is the ratio of air to water density. We define a form drag coefficient dependent on significant wave height $H_S = 4(E_T/g)^{1/2}$—where E_T is total wave energy—and inverse wave age, $\sigma_P U_{10}/g$; σ_P is frequency at the peak of the wave spectrum, U_{10} is the 10-m wind speed; and $\kappa = 0.41$ is the von Kármán constant. Thus,

$$C_{DP} = \left[\frac{\kappa}{\ln(10\,\text{m}/z_{0P})}\right]^2 \quad \text{and} \tag{21a}$$

$$z_{0P} = 1.38 \times 10^{-4} H_S \left(\frac{\sigma_P U_{10}}{g}\right)^{2.66} \tag{21b}$$

(Donelan et al. 1985, 1992; Hwang and Wang 2004). For turbulent flow over a smooth surface, the friction drag coefficient is

$$C_{DT} = \left[\frac{\kappa}{\ln(10\,\text{m}/z_{0T})}\right]^2 \quad \text{and} \tag{22a}$$

$$z_{0T} = 0.18\nu/u_* \tag{22b}$$

(Schlicting 1979) and is appropriate to turbulent flow with no waves and therefore involves the kinematic viscosity ν. Of the two determinations, C_{DP} and C_{DT}, the maximum as calculated in (21) and (22) prevails; the other is set to zero. In practice, the turbulence formula, (21b), is only invoked for low wind speeds and has very little influence on calculated results.

The switch from C_{DT} to C_{DP} or vice versa might seem abrupt but in Schlicting (1979, Fig. 20.21) it is seen that, for rough walls, an abrupt change is a plausible approximation. Given the current state of knowledge, the approximation for wavy walls is appropriately simple and is approximately justified by most drag coefficients plotted as a function of wind speed (see Fig. 3, described in greater detail below). However, the correct partition between form drag and friction drag is an outstanding research question (e.g., Janssen 1989; Donelan et al. 2012).

b. The temperature equation

The equation for potential temperature is

$$\frac{\partial T}{\partial t} = \frac{\partial Q}{\partial z} + \frac{\partial R}{\partial z}, \tag{23}$$

where R is the solar penetrative radiation flux. The turbulence-based heat flux (pressure is absent in scalar equations and so is pressure–slope transfer) is

$$Q = K_H \frac{\partial T}{\partial z}, \tag{24}$$

where K_H is a mixing coefficient for heat flux defined below.

c. The turbulence kinetic energy equation

The turbulence kinetic energy equation is

$$\frac{\partial q^2}{\partial t} = \frac{\partial}{\partial z}\left(K_q \frac{\partial q^2}{\partial z}\right) + 2(\tau_{P\alpha} + \tau_{T\alpha})\left(\frac{\partial U_\alpha}{\partial z}\right) - 2K_H \frac{g}{\rho_0}\frac{\partial \rho}{\partial z} - \frac{q^3}{\Lambda_1}, \tag{25}$$

q^2 is twice the turbulence energy, and K_q is its mixing coefficient. The second, third, and fourth terms on the right-hand side are shear production, buoyancy production, and dissipation, respectively; $\Lambda_1 = 16.6\ell$ and ℓ is a length scale discussed below. It is noted that the shear source term $(\tau_{P\alpha} + \tau_{T\alpha})\partial U_\alpha/\partial z$ is derived by consideration of the mean kinetic energy equation obtained by multiplying (16) by U_α (Mellor 2005); the term appears as a sink term that requires balance of a source term in the turbulence kinetic energy equation and thus includes $\tau_{P\alpha}$ as well as the usual $\tau_{T\alpha}$.

The surface boundary condition for the turbulence equation is as originally suggested by Craig and Banner (1994), whereby a source of turbulence due to wave breaking is injected at the surface as a surface boundary condition as in

$$K_q \frac{\partial q^2}{\partial z}\bigg|_{z=0} = \int_{-\pi}^{\pi} S_{\theta S_{\text{dis}}}\, d\theta, \tag{26}$$

where $S_{\theta S_{\text{dis}}}$ is obtained from the wave model described in the next section; see Mellor and Blumberg (2004) for numerical details. In those papers, a wave model was not available and breaking wave energy was simply parameterized by αu_*^3, where u_* is the friction velocity and $\alpha \cong 100$. Until research provides a means of vertically distributing $\int_{-\pi}^{\pi} S_{\theta S_{\text{dis}}}\, d\theta$ into the subsurface layers of the water column, (26) is regarded as an approximation.

Considering the length scale, an important aspect here is that, near the surface, we set

$$\ell = \max(\ell_0, \ell_z), \tag{27}$$

where ℓ_z is the conventional length scale for which there are many prescriptions in the literature, reflecting a high degree of empiricism, but, generally, $\ell_z \sim \kappa z$ as $z \to 0$. Here, ℓ_z is obtained from a differential equation (Mellor and Yamada 1982). An algebraic equation would undoubtedly work well if it is tuned to the ocean surface layer case. It has been assumed by Terray et al. (1999) that $\ell_0 \propto H_S$ where the proportionality constant is a tuning constant for which solutions are quite sensitive (Mellor and Blumberg 2004). To best fit the data in Fig. 4 (described in greater detail below), we have set $\ell_0 = H_S$; no significance is attached to the proportionality constant of unity. In three-dimensional simulations where internal waves, surface cyclonic divergences, or anticyclonic convergences are in play, mixing is enhanced and the proportionality coefficient may have to be decreased.

d. The mixing coefficients

The model is completed by

$$(K_M, K_H, K_q) = (S_M, S_H, S_q)\ell q, \tag{28}$$

where the stability factors S_M and S_H are functions of $(\rho_0 q^2)^{-1}\ell^2 g\partial\rho/\partial z$ as originally derived by Mellor and Yamada (1982) and modified by Galperin et al. (1988). We have in the past vacillated in specifying S_q, either making it proportional to S_H or setting it equal to a constant. The resulting differences are small but here we choose $S_q = 0.2$.

From the above, it will be seen that wave information is required. Specifically, the significant wave height and wave age is needed in (21) and the vertical dependence of the momentum pressure transfer in (17) requires the peak wavenumber.

e. The wave model

We invoke the phase-averaged, nonlinear wave model of MDO. The model is based on a parameterization of the shape of the frequency spectrum according to Donelan et al. (1985) so that one deals with the wave energy E_θ dependent on wave propagation direction θ, the horizontal coordinates, and time. It is, therefore, a relatively simple model compared to third-generation models. However, it has been shown in MDO to reproduce fetch- and duration-limited data and to produce comparable performance to Simulated Waves Nearshore (SWAN; Booij and Holthuijsen 1999) in comparison with buoy data during Hurricane Katrina. It is well suited to present requirements in that it is computationally efficient (requiring two orders of magnitude less computational resource relative to third-generation models) and is comparable to surface boundary layer models in that details of both wave spectra and turbulence spectra are avoided.

The wave energy equation, greatly simplified by exclusion of horizontal gradients, is

$$\frac{\partial E_\theta}{\partial t} = S_{\theta_{\text{in}}} - S_{\theta_{\text{out}}} - S_{\theta S_{\text{dis}}}, \tag{29}$$

where E_θ is the energy of waves propagating in direction θ. Here, wave direction is the only independent variable; advective and refractive terms—otherwise included in MDO—disappear. Wave variables are distributed in the range $-\pi < \theta \le \pi$. We next define a spreading function

$$f_{\text{spr}} \equiv \begin{cases} \frac{\beta}{2}\text{sech}^2[\beta(\theta - \theta_W)]; & |\theta - \theta_W| \le \pi/2 \\ 0; & |\theta - \theta_W| > \pi/2 \end{cases}. \tag{30}$$

The wind direction is θ_W and $\beta = 2.2$. Thus, f_{spr} is at a maximum in the wind direction and diminishes on either side of the wind direction.

The wind source term $S_{\theta_{\text{in}}}$ is the usual wind input for waves propagating in a direction near the wind; as determined in MDO, it is

$$S_{\theta_{\text{in}}}/u_{*P}^3 = 370\exp(-0.33U_{10}\sigma_P/g)f_{\text{spr}}(\theta, \theta_W), \tag{31a}$$

where $u_{*P} = |\tau_{P\alpha}(0)|^{1/2}$ is the water-side friction velocity. Recall that $U_{10}\sigma_P/g$ ($= U_{10}/c_P$ for deep water, and c_p is the peak spectral phase speed) is the inverse wage age. A second sink term

$$S_{\theta_{\text{out}}}/u_{*P}^3 = 370\exp(-0.33U_{10}\sigma_P/g)0.4f_{\text{spr}}(\theta, \theta_W + \pi) \tag{31b}$$

accounts for waves propagating in directions opposite to the wind direction. The factor, 0.4, is according to Donelan (1999). Only positive E_θ is permitted; therefore, after E_θ is reduced to zero in the vicinity of $\theta = \theta_W + \pi$, (31b) is ineffective.

The surface wave dissipation is given by

$$S_{\theta S_{\text{dis}}} = aS_{\theta_{\text{in}}} + bE_\theta\sigma_P \tag{32}$$

where $a = 0.925$ was determined empirically in MDO by reference to fetch data and $b = 0.18 \times 10^{-4}$ is determined by the limiting case $\partial E_\theta/\partial t = 0$. The first term in (32) represents the fact that the high-frequency part of the spectrum is dissipated very nearly in situ and the second part is dissipation of the middle- ($\sigma \approx \sigma_P$) to low-frequency part of the spectrum. This means, of course, that overall wave growth only responds to $(1 - a)S_{\theta_{\text{in}}} - bE_\theta\sigma_P$; nevertheless, the full dissipation is needed as input to the turbulence kinetic energy equation as in (26). The model crudely approximates swell by using a reduced $b = (0.18 \times 10^{-4})/5$ when $u_{*P} = 0$.

Most of the wind input energy is dissipated in situ. Aside from its wave age dependence, (31a) resembles the dissipation suggested by Craig and Banner (1994) after integration over all wave angles.

A θ-dependent frequency equation, simplified for horizontally homogeneous flow, is

$$\frac{\partial \sigma_\theta}{\partial t} = -\Re \quad \text{and} \tag{33a}$$

$$\Re = \sigma_P(\sigma_P - \sigma_\theta)f_{\text{spr}}^{1/2}. \tag{33b}$$

In regions of θ that are wind driven ($f_{\text{spr}} > 0$), the source term $\Re$ has the effect of nudging (a term used, for example, in data assimilation of various ocean properties) σ_θ toward σ_P; where waves are not wind driven, $f_{\text{spr}} = 0$ and σ_θ is unchanged. The peak frequency is then parameterized by

$$U_{10}\sigma_P/g = (C_\sigma U_{10}^4/gE_{TW})^{0.303} \tag{34}$$

as determined by Donelan et al. (1985, 1992) and Hwang and Wang (2004). The constant C_σ is 0.0022. Although based mostly on moderate winds, (34) has also been shown to conform to hurricane data by Young (2006). Here, $E_{TW} = \int E_\theta\, d\theta$ is the integral over wave angle but limited to the wind-driven portion, where $f_{\text{spr}} > 0$; E_T is the same integral but taken over all wave angles.

The Stokes drift for a monochromatic wave in deep water is $u_{S\alpha} = 2k_\alpha(E/c)\exp(2kz)$ where the wavenumber vector is $k_\alpha = k(\cos\theta, \sin\theta)$ and $k_\alpha^2 = k^2$. Because wave properties are distributed in the range $-\pi < \theta < \pi$, an average is

$$(u_{Sx}, u_{Sy}) = \int_{-\pi}^{\pi} (\cos\theta, \sin\theta)\frac{2k_\theta}{c_\theta}E_\theta \exp(2k_\theta z)\, d\theta. \tag{35}$$

5. Station Papa data

We now appeal to the data from Weather Station Papa (50°N, 145°W) analyzed by Martin (1985) for the year 1966. The wind stress is as described above but the heat flux at the surface is that calculated by Martin using climatological radiation and conventional bulk surface formulas. The vertical distribution of ocean velocities and attendant variables on the one-dimensional grid, $-200 < z < 0$, includes 40 evenly distributed grid points except for the topmost 7 points that are logarithmically distributed. The wave variables are on the grid $-\pi < \theta \le \pi$

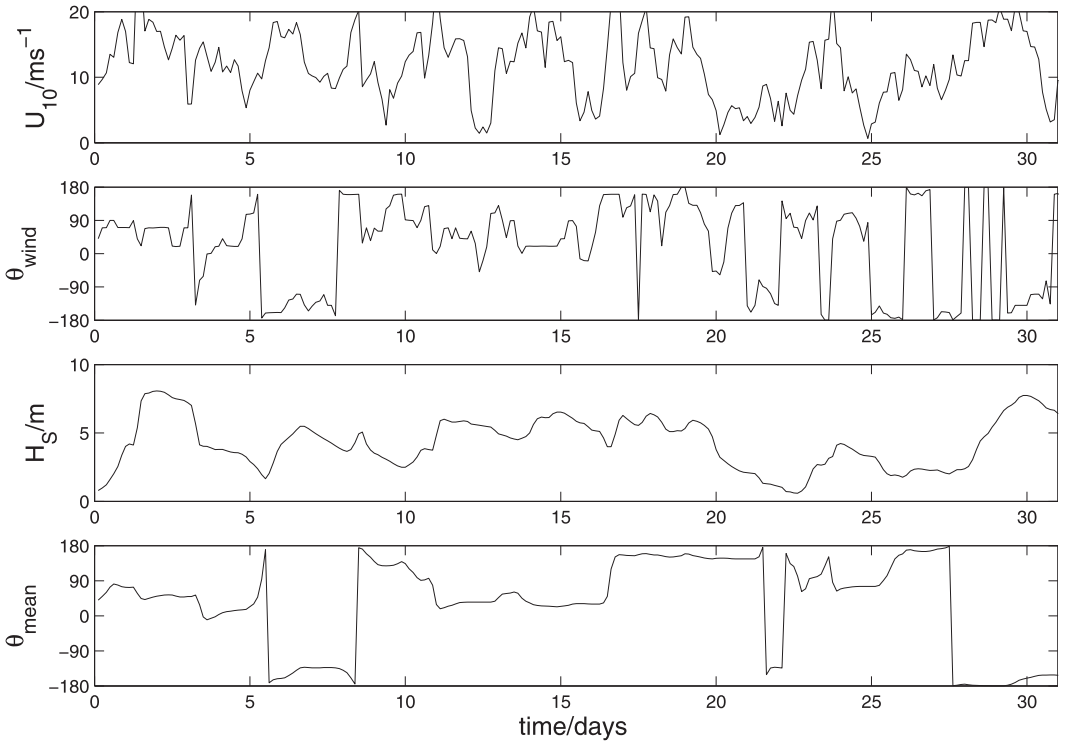

FIG. 2. Time series of the first 31 days of a yearlong simulation of weather station Papa for 1961. (top) Wind speed ($\mathrm{m\,s^{-1}}$) and direction (°) from Martin (1985) are shown. (bottom) Calculated significant wave height H_S (m) and mean wave propagation direction $\overline{\theta} = \theta_{\mathrm{mean}}$ (°) are shown.

and are divided into 24 equally spaced increments. The time step is 5 min.

A time series for wind speed and direction are plotted in the top two panels in Fig. 2, and the calculated significant wave height and mean wave propagation direction are shown in the bottom panels for the month of January when the winds are quite strong.

Figure 3 is a conventional plot of drag coefficient versus wind speed sampled at 3-h intervals in January. The scatter is due to the dependency of C_D on significant wave height and wave age in (21); nevertheless, it is somewhat remarkable that a complicated path through the wave variables and (21) should closely adhere to the simple $C_D(U_{10})$.

Figure 4 presents sample profiles of current $\hat{u}_x$ and $\hat{u}_y$ and Stokes drift u_{Sx} and u_{Sy} components. The total mean velocity components U_x and U_y are the sum of the two. The narrow southward jet around $z = -110$ m—akin to the nocturnal jet in the atmosphere—is the result of an upward progression of the interface from unstable forced to stable unforced portions of the water column.

In Fig. 5 are sample plots of $\tau_{P\alpha}$ and $\tau_{T\alpha}$ at day 30; notice that $\tau_{T\alpha}$ is nil at the surface but comparable to $\tau_{P\alpha}$ below the surface.

Figure 6 compares station Papa yearlong temperature data with calculations. The short-wave motion, presumably internal waves, is missing; otherwise the comparison is quite favorable. Finally, the station Papa monthly-averaged surface temperature is compared

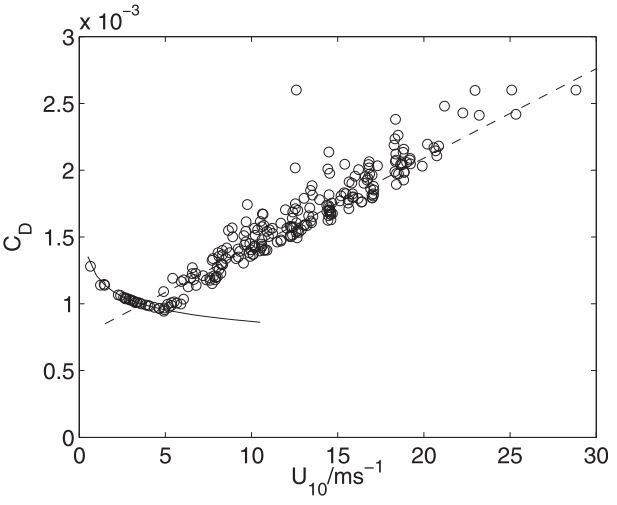

FIG. 3. C_D sampled at 3-h intervals for the first 31 days. The solid line is from (22) and the dashed line is the linear relation $(0.75 + 0.067U_{10})10^{-3}$ from Garrett (1977).

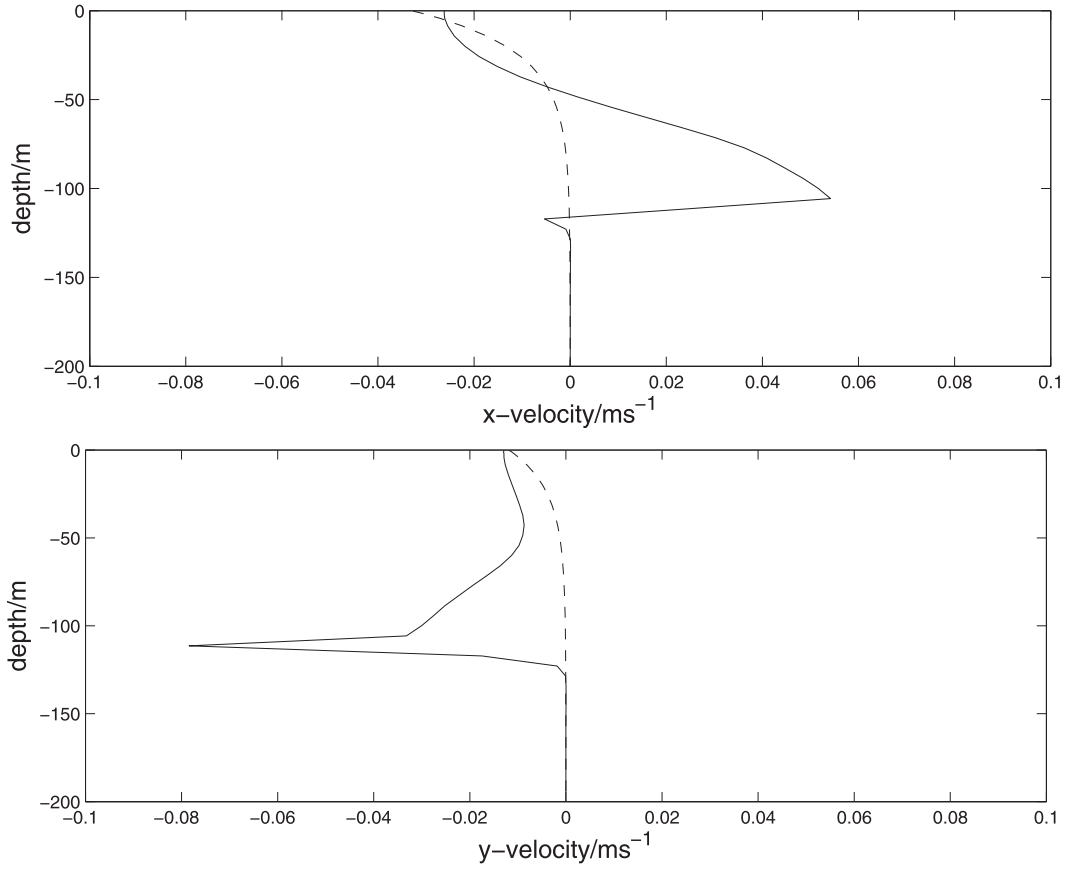

FIG. 4. Sample velocity (m s^{-1}) profiles at day 30 of the yearlong computation. The solid lines are the currents and the dashed lines are Stokes drifts. (top) The eastward and (bottom) northward components are shown.

with data in Fig. 7 in the manner presented by Martin (1985).

6. The generation of Stokes drift and Eulerian current

To simplify understanding of the detailed physics of the generation of Stokes drift $u_{S\alpha}$ and current $\hat{u}_\alpha$, let $f = c_R = 0$ and integrate (16) so that

$$\frac{\partial}{\partial t}(M_{S\alpha} + \hat{M}_\alpha) = \tau_{P\alpha}(0), \tag{36}$$

where $M_{S\alpha} \equiv \int_{-h}^{0} u_{S\alpha}\, dz$ and $\hat{M}_\alpha \equiv \int_{-h}^{0} \hat{u}_\alpha\, dz$. As in section 4, assume that form drag $\tau_{P\alpha}(0)$ is the dominant surface wind stress. For monochromatic waves, it can be shown that $E = E_T = c_\alpha M_{S\alpha}$ whereas for a spectrum, following Terray et al. (1996), we let $E = \overline{c}_\alpha M_{S\alpha}$, where $\overline{c}_\alpha$ is a spectral average. Now, as in familiar numerical implementations, conceptually time split the forcing and dissipative processes. For the first time step, the forcing process, the total energy (29) with no dissipation, converts to $\partial \overline{c}_\alpha M_{S\alpha}/\partial t = S_{\text{in}}$. Thus, according to the energy equation, only Stokes drift is created and from (36) $\overline{c}_\alpha \tau_{P\alpha} = S_{\text{in}}$. For the second time step, the dissipative process is $\partial \overline{c}_\alpha M_{S\alpha}/\partial t = -S_{\text{dis}}$ but $\partial(M_{S\alpha} + \hat{M}_\alpha)/\partial t = 0$. Thus, the Stokes drift decreases and is converted into current. Appendix B discusses the relation $\overline{c}_\alpha \tau_{P\alpha} = S_{\text{in}}$ in more detail.

Reinstating f, a third time step can accommodate changes due to the Coriolis term.

7. Summary

In this paper, momentum transfer into an oceanic water column via pressure acting on material wave surfaces is demonstrated by a phase-resolved analytical model simplified by excluding currents, turbulence, and horizontal variability. The results are phase averaged and partially account for terms in a more complete model.

There then followed a description of a phase-averaged model complete with waves coupled to an ocean surface boundary layer model wherein momentum and energy is

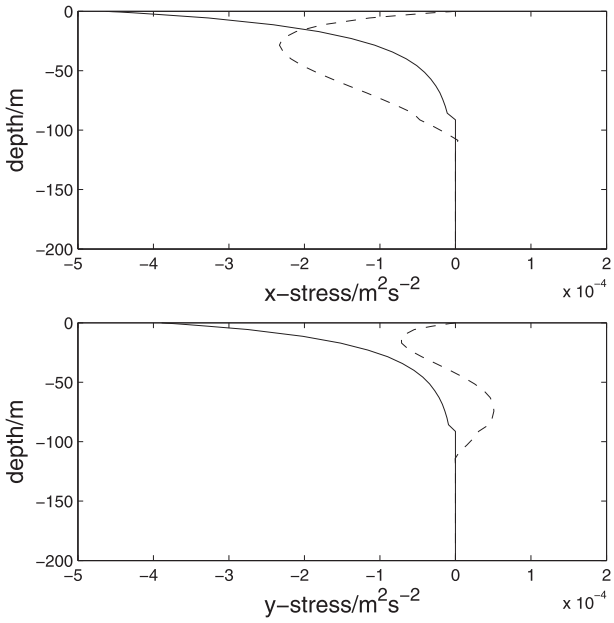

FIG. 5. Sample stress profiles at day 30 of the yearlong computation. The solid lines are the pressure transfer of momentum into the water column according to (17); the dashed lines are the turbulence transfers according to (18). (top) The eastward and (bottom) northward components are shown.

transferred to and from waves and the underlying water column.

We then compared with the data of Martin (1985), a well-known and much-cited dataset. Other data are included in Mellor (2001) and experience indicates that a model that performs well with the Martin data also does well generally. It is unfortunate that concomitant surface wave data are not available to compare with the calculated data. But as noted above, the wave model has reproduced fetch- and duration-limited data and hurricane buoy data so it is presumed that the calculated wave properties are reasonable. However, the main focus of the paper is on coupling waves to surface boundary layer dynamics and on the combined but separate role of turbulence- and pressure–slope-supported stresses as demonstrated in Fig. 5.

It is noted that there are no adjustable constants in the Mellor–Yamada turbulence closure model, which covers many different flow problems. However, with the addition of surface gravity waves, an adjustable constant is introduced in the relation $\ell_0 = H_S$, where, as stated above, the constant is unity. The model has been run excluding pressure–slope transfer reverting to the more conventional turbulence transfer. Consequently, the summertime temperatures are reduced by about a degree. Now, if ℓ_0 is adjusted so that $\ell_0 = 0.85H_S$, the comparison (not shown) between measured data and calculations is nearly the same as in Fig. 7. (Most of the year, velocity profiles are nearly the same but do differ significantly during summer months.) Therefore, the good agreement in Fig. 7 does not justify inclusion of pressure–slope per se. Justification derives from the simple fact that pressure–slope transfer into the water column is the logical continuation of form drag, which is nomenclature for pressure–slope transfer at the surface. Otherwise, form drag would be discontinuously continued into the water column by turbulence transfer.

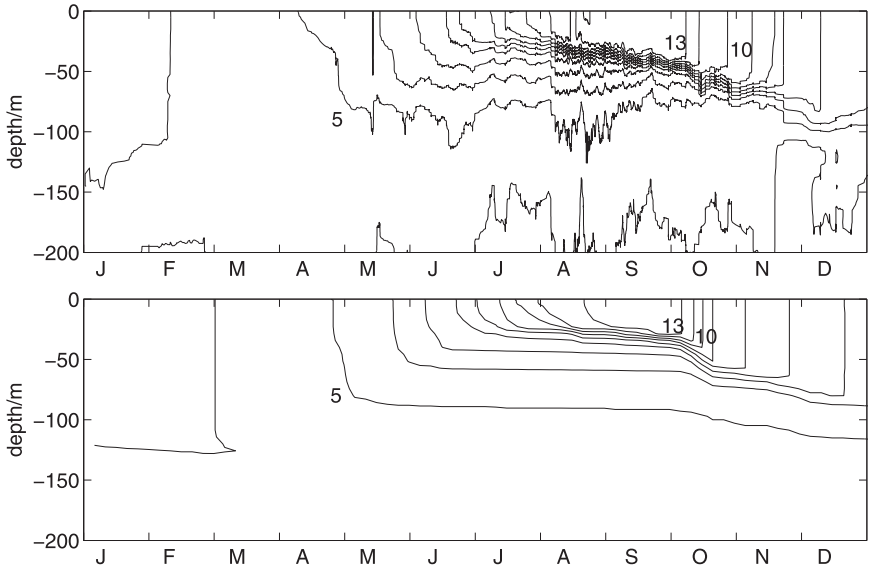

FIG. 6. The yearlong temperatures (°C; contour interval is 1°C) at station Papa. (top) The measured and (bottom) calculated values are shown.

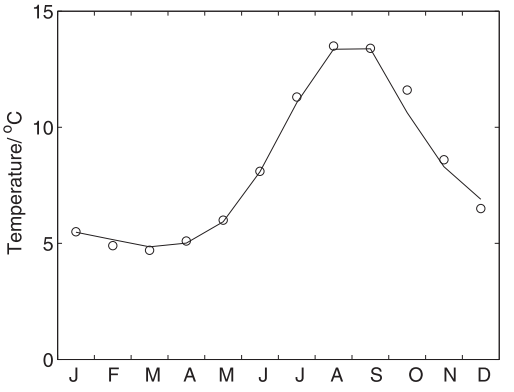

FIG. 7. The yearlong surface temperatures (°C) averaged monthly. The circles are measured and the solid lines are calculated values.

Scientific progress does require improved physical description and understanding of oceanic processes whenever possible.

Acknowledgments. Two reviewers made important suggestions that improved the paper.

APPENDIX A

Derivation of (11)

Despite the simplicity of (11), its derivation is rather complicated but simpler than that in Mellor (2003) in that currents are nil ($\hat{u} = 0$). Thus, it can serve the purpose of providing an introduction to the methodology of the 2003 paper; that paper of course contains more realism than does the idealized Rayleigh drag as shown in section 2.

Here, (2a) is transformed according to

$$\varphi(x, z, t) \rightarrow \varphi(x, \varsigma, t), \tag{A1}$$

where

$$z = \varsigma + \tilde{s} \quad \text{and} \tag{A2a}$$

$$\tilde{s} = a\frac{\sinh k(h+\varsigma)}{\sinh kh}\cos\psi, \tag{A2b}$$

and u or p is represented by φ. Surfaces of constant $\varsigma + \tilde{s}$ are material surfaces, whereas surfaces of constant ς are fixed, time-independent (rest) surfaces. From the expression for the vertical velocity $\tilde{w}$ below, one sees that $\tilde{s}$ derives from $\partial\tilde{s}/\partial t = \tilde{w}$. At $\varsigma = 0, z = \tilde{s}(0) = \eta = a\cos\psi$, whereas at $\varsigma = -h, z = -h$. From (A2a) and (A2b), useful relations are

$$z_\varsigma = 1 + \tilde{s}_\varsigma \quad \text{and} \tag{A3a}$$

$$\tilde{s}_\varsigma = ka\frac{\cosh k(h+\varsigma)}{\sinh kh}\cos\psi. \tag{A3b}$$

Now, following Mellor (2003), derivatives of u and p transform according to

$$\frac{\partial u}{\partial t} \rightarrow \frac{\partial u}{\partial t} - \frac{\partial u}{\partial \varsigma}\frac{z_t}{z_\varsigma} \quad \text{and} \tag{A4a}$$

$$\frac{\partial p}{\partial x} \rightarrow \frac{\partial p}{\partial x} - \frac{\partial p}{\partial \varsigma}\frac{z_x}{z_\varsigma}. \tag{A4b}$$

so that (2a) may be transformed to

$$z_\varsigma\frac{\partial u}{\partial t} - \frac{\partial u}{\partial \varsigma}z_t + z_\varsigma\frac{\partial p}{\partial x} - \frac{\partial p}{\partial \varsigma}z_x = -rz_\varsigma u.$$

After rearranging

$$\frac{\partial uz_\varsigma}{\partial t} - \frac{\partial uz_t}{\partial \varsigma} + \frac{\partial pz_\varsigma}{\partial x} - \frac{\partial pz_x}{\partial \varsigma} = -rz_\varsigma u. \tag{A5}$$

The equations for wave velocity,

$$u = kac\frac{\cosh k(h+z)}{\sinh kh}\cos\psi \quad \text{and} \tag{A6a}$$

$$w = kac\frac{\sinh k(h+z)}{\sinh kh}\sin\psi, \tag{A6b}$$

are exact irrotational solutions (Mellor 2011) to (1) and (2) in the region $-h < z < \eta(x, t)$. Thus, recalling (A2a), $u = [kac\cosh k(h + \varsigma + \tilde{s})/\sinh kh]\cos\psi$, one has

$$u = \tilde{u} + \frac{\partial\tilde{u}}{\partial\varsigma}\tilde{s} \quad \text{and} \tag{A7a}$$

$$\tilde{u} \equiv kac\frac{\cosh k(h+\varsigma)}{\sinh kh}\cos\psi \tag{A7b}$$

and also

$$w = \tilde{w} + \frac{\partial\tilde{w}}{\partial\varsigma}\tilde{s} \quad \text{and} \tag{A7c}$$

$$\tilde{w} \equiv kac\frac{\sinh k(h+\varsigma)}{\sinh kh}\sin\psi \tag{A7d}$$

plus terms higher order in ka. Similarly (9) becomes

$$p = -gz + ga\frac{\cosh k(h+\varsigma+\tilde{s})}{\cosh kh}\cos\psi + p_w\frac{\cosh k(h+\varsigma+\tilde{s})}{\cosh kh} \tag{A8}$$

or

$$p = \tilde{p} + \frac{\partial\tilde{p}}{\partial\varsigma}\tilde{s} + p_w\frac{\cosh k(h+\varsigma)}{\cosh kD} \quad \text{and} \tag{A9a}$$

$$\tilde{p} = -g\varsigma + ga\frac{\cosh k(h+\varsigma)}{\cosh kD}\cos\psi. \qquad \text{(A9b)}$$

The phase average of (A5) is

$$\frac{\partial \overline{uz_\varsigma}}{\partial t} - \frac{\partial \overline{pz_x}}{\partial \varsigma} = -r\overline{z_\varsigma u}, \qquad \text{(A10)}$$

where, for horizontal homogeneity, the term $\partial\overline{pz_\varsigma}/\partial x = 0$; also, u and z_t are uncorrelated $\overline{uz_t} = 0$. Henceforth, the terms, F_{CC} and F_{SS}, defined in sections 2 and 3, will be used. Now from (A2), $z_x = -kaF_{SS}\sin\psi$ so that

$$\overline{pz_x} = -\overline{p_w F_{CC} kaF_{SS}\sin\psi} = \overline{p_w \frac{\partial\eta}{\partial x}} F_{CC}F_{SS}$$

because $p_w \propto \sin\psi$ and $\partial\eta/\partial x = ka\sin\psi$ whereas the other terms in (A9a) are not correlated. The other term in (A10) is

$$\overline{z_\varsigma u} = \overline{(1+s_\varsigma)\left(\tilde{u} + \frac{\partial\tilde{u}}{\partial\varsigma}\tilde{s}\right)} = \frac{\overline{\partial\tilde{u}\tilde{s}}}{\partial\varsigma} = \frac{E}{c}\frac{\partial}{\partial\varsigma}\ F_{CC}F_{SS} = u_S,$$

where (8) and $E = ga^2$ are used. Therefore (A10) becomes

$$\frac{\partial u_S}{\partial t} = \frac{\partial\tau_P}{\partial\varsigma} - ru_S \qquad \text{(A11)}$$

as in (11).

The key to the above derivation is that phase averaging $\overline{(\,)} = L^{-1}\int_0^L (\,)\,dx$ is processed after the independent variables are transformed to x and the fixed ς.

APPENDIX B

The Relation $\overline{c}_\alpha\tau_{P\alpha} = S_{\text{in}}$

Using (31a), (19), (21a), and (21b), one obtains

$$\frac{\overline{c}}{c_P} = 370(\varepsilon C_D)^{1/2}Ae^{-0.33A} \quad \text{and} \qquad \text{(B1a)}$$

$$\frac{u_{*a}}{c_P} = C_D^{1/2}A, \qquad \text{(B1b)}$$

where $A = U_{10}\sigma_P/g$ is the inverse wave age and u_{*a} is the air side friction velocity. Here, (B1a) and (B1b) are expressions reflecting different curve-fitted empirical expressions. Terray et al. (1996) used measured spectra and performed an integration over spectral frequency to determine $\overline{c}$. They plotted $\overline{c}/c_P$ versus u_{*a}/c_P and the variables in (B1) and Fig. B1 are chosen to conform to their choice of variables. Here, C_D is determined using the Garrett relation cited in Fig. 3. The reader is referred to their Fig. 6 and it will be seen that Fig. B1 is a reasonable representation of their Fig. 6; the greatest discrepancy is noted for small values of u_{*a}/c_P. The range of $5 \le U_{10} \le 15$ covers the range of their dataset and approximately brackets the scatter in their Fig. 6.

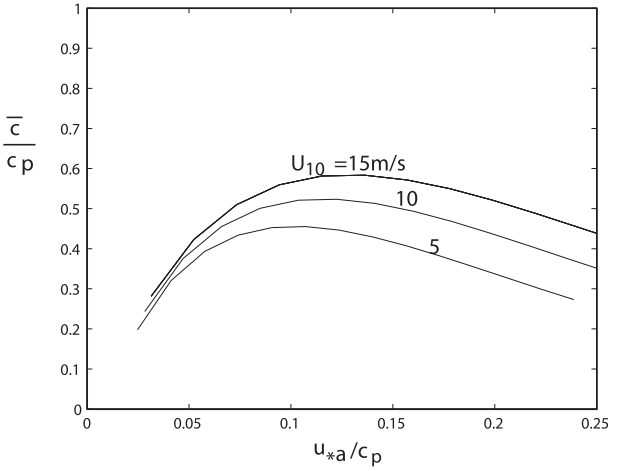

FIG. B1. The relation between $\overline{c}/c_P$ vs inverse wave age to be compared with a similar plot in Terray et al. (1996).

REFERENCES

Booij, N., R. C. Ris, and L. H. Holthuijsen, 1999: A third-generation wave model for coastal regions: 1. Model description and validation. *J. Geophys. Res.,* **104** (C4), 7649–7666.

Buckles, J., T. J. Hanratty, and R. Adrian, 1984: Turbulent flow over large-amplitude wavy surfaces. *J. Fluid Mech.,* **140,** 27–44.

Craig, P. D., and M. L. Banner, 1994: Modeling wave-enhanced turbulence in the ocean surface layer. *J. Phys. Oceanogr.,* **24,** 2546–2559.

Donelan, M. A., 1999: Wind-induced growth and attenuation of laboratory waves. *Wind-over-Wave Couplings,* S. G. Sajjadi, N. H. Thomas, and J. C. R. Hunt, Eds., Clarendon Press, 183–194.

——, J. Hamilton, and W. H. Hui, 1985: Directional spectra of wind-generated waves. *Philos. Trans. Roy. Soc. London,* **A315,** 509–562.

——, M. Skafel, H. Graber, P. Liu, D. Schwab, and S. Venkates, 1992: On the growth of wind-generated waves. *Atmos.–Ocean,* **30,** 457–478.

——, M. Curcic, S. S. Chen, and A. K. Magnusson, 2012: Modeling waves and wind stress. *J. Geophys. Res.,* **117,** C00J23, doi:10.1029/2011JC007787.

Galperin, B., L. H. Kantha, S. Hassid, and A. Rosatiu, 1988: A quasi-equilibrium turbulent energy model for geophysical flows. *J. Atmos. Sci.,* **45,** 55–62.

Garrett, J. R., 1977: Review of drag coefficients over oceans and continents. *Mon. Wea. Rev.,* **105,** 915–929.

Hwang, P. A., 2006: Duration and fetch-limited growth functions and wind-generated waves parameterized with three different scaling wind velocities. *J. Geophys. Res.,* **111,** C02005, doi:10.1029/2005JC003180.

——, and D. W. Wang, 2004: Field measurements of duration-limited growth of wind-generated ocean surface waves at young stage of development. *J. Phys. Oceanogr.,* **34,** 2316–2326.

Janssen, P. A. E. M., 1989: Wave-induced stress and the drag of air flow over sea waves. *J. Phys. Oceanogr.,* **19,** 745–754.

Large, W. G., J. C. McWilliams, and S. C. Doney, 1994: Oceanic vertical mixing: A review and a model with nonlocal boundary layer parameterization. *Rev. Geophys.,* **32,** 363–403.

Martin, P. J., 1985: Simulation of the mixed layers at OWS November and Papa with several models. *J. Geophys. Res.,* **90,** 903–916.

Mellor, G. L., 2001: One-dimensional, ocean surface layer modeling: A problem and a solution. *J. Phys. Oceanogr.,* **31,** 790–809.

——, 2003: The three-dimensional, current, and surface wave equations. *J. Phys. Oceanogr.,* **33,** 1978–1989.

——, 2005: Some consequences of the three-dimensional current and surface wave equations. *J. Phys. Oceanogr.,* **35,** 2291–2298.

——, 2011: Wave radiation stress. *Ocean Dyn.,* **61,** 563–568.

——, 2013: Waves, circulation, and vertical dependence. *Ocean Dyn.,* **63,** 447–457.

——, and T. Yamada, 1982: Development of a turbulence closure model for geophysical fluid problems. *Rev. Geophys. Space Phys.,* **20,** 851–875.

——, and A. Blumberg, 2004: Wave breaking and ocean surface layer thermal response. *J. Phys. Oceanogr.,* **34,** 693–698.

——, M. A. Donelan, and L.-Y. Oey, 2008: A surface wave model for coupling with numerical ocean circulation models. *J. Atmos. Oceanic Technol.,* **35,** 1785–1807.

Pollard, R. T., and R. C. Millard, 1970: Comparisons between observed and simulated wind-generated inertial oscillations. *Deep-Sea Res.,* **17,** 813–821.

Schlicting, H., 1979: *Boundary Layer Theory.* 7th ed. McGraw-Hill, 817 pp.

Snodgrass, F. E., G. W. Groves, K. Hasselmann, G. R. Miller, W. H. Munk, and W. H. Powers, 1966: Propagation of swell across the Pacific. *Philos. Trans. Roy. Soc. London,* **259,** 431–497.

Terray, E. A., M. A. Donelan, Y. C. Agrawal, W. M. Drennan, K. K. Kahma, A. J. Williams III, P. A. Hwang, and S. A. Kitaigorodskii, 1996: Estimates of kinetic energy dissipation under breaking waves. *J. Phys. Oceanogr.,* **26,** 792–807.

——, W. M. Drennan, and M. A. Donelan, 1999: The vertical structure of shear and dissipation on the ocean surface layer. *The Wind-Driven Air–Sea Interface,* School of Mathematics, University of New South Wales, 239–245.

Young, I. R., 2006: Directional spectra of hurricane wind waves. *J. Geophys. Res.,* **111,** C08020, doi:10.1029/2006JC003540.